Supplementary figures:

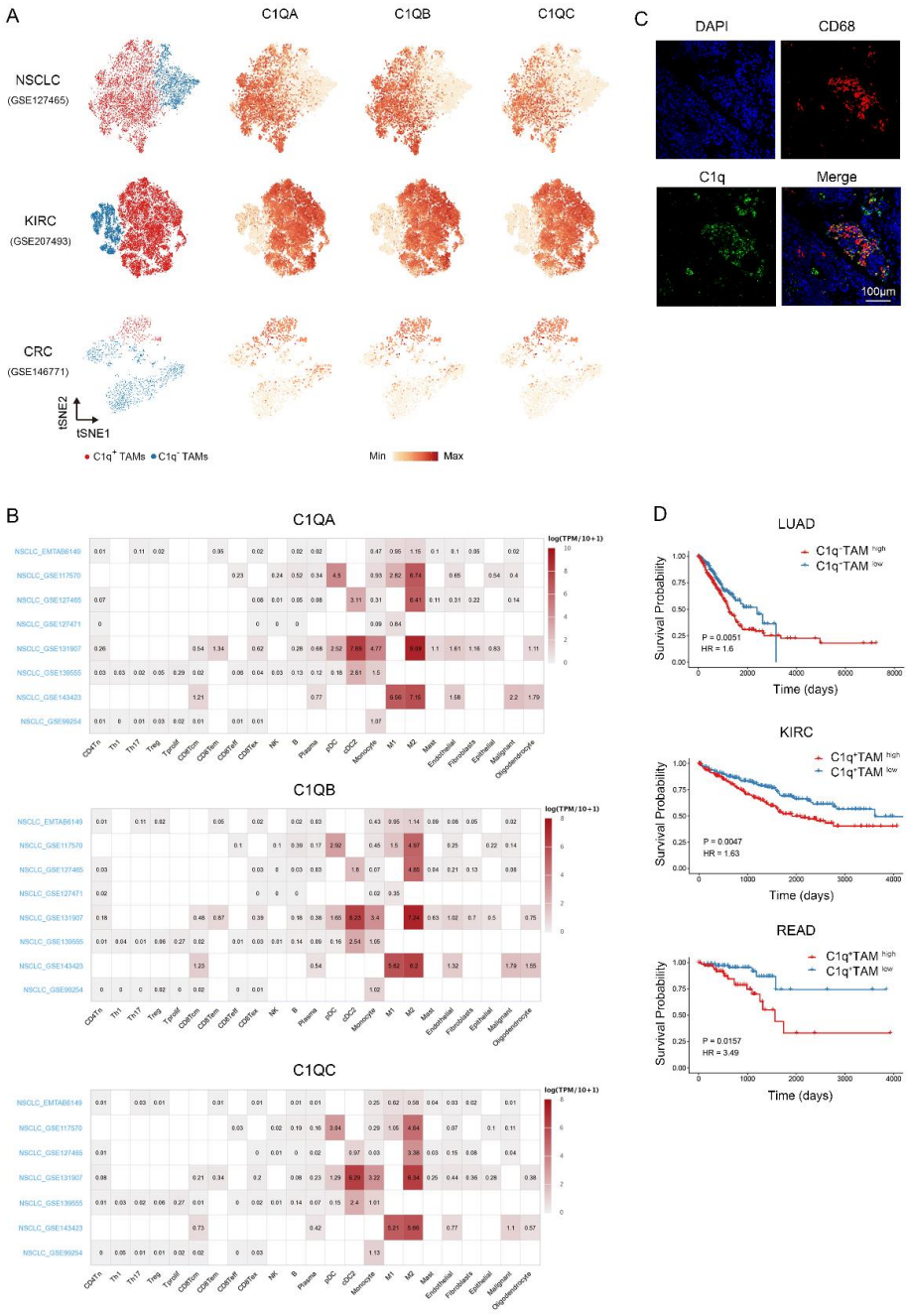

Figure S1. Related to Figure 1.

(A) The publicly available scRNA-seq data were analyzed, and the gene expression of C1QA, C1QB, and C1QC was demonstrated in t-distributed stochastic neighbor embedding (t-SNE) space

for non-small-cell lung cancer (NSCLC), kidney renal clear cell carcinoma (KIRC), and colorectal cancer (CRC).

(B) Gene expression of C1QA, C1QB and C1QC in various cell subpopulations of lung cancer was analysis using the Tumor Immune Single-cell Hub (TISCH) database (http://tisch.comp-genomics.org).

(C) IF staining of C1q and CD68 in human lung cancer tissue. Red, CD68; green, C1q; and blue, DAPI for nucleus. Scale bar 100 μm.

(D) The Kaplan-Meier curve showed the overall survival proportion of lung adenocarcinoma (LUAD), KIRC, and rectum adenocarcinoma (READ) based on publicly available scRNA-seq data.

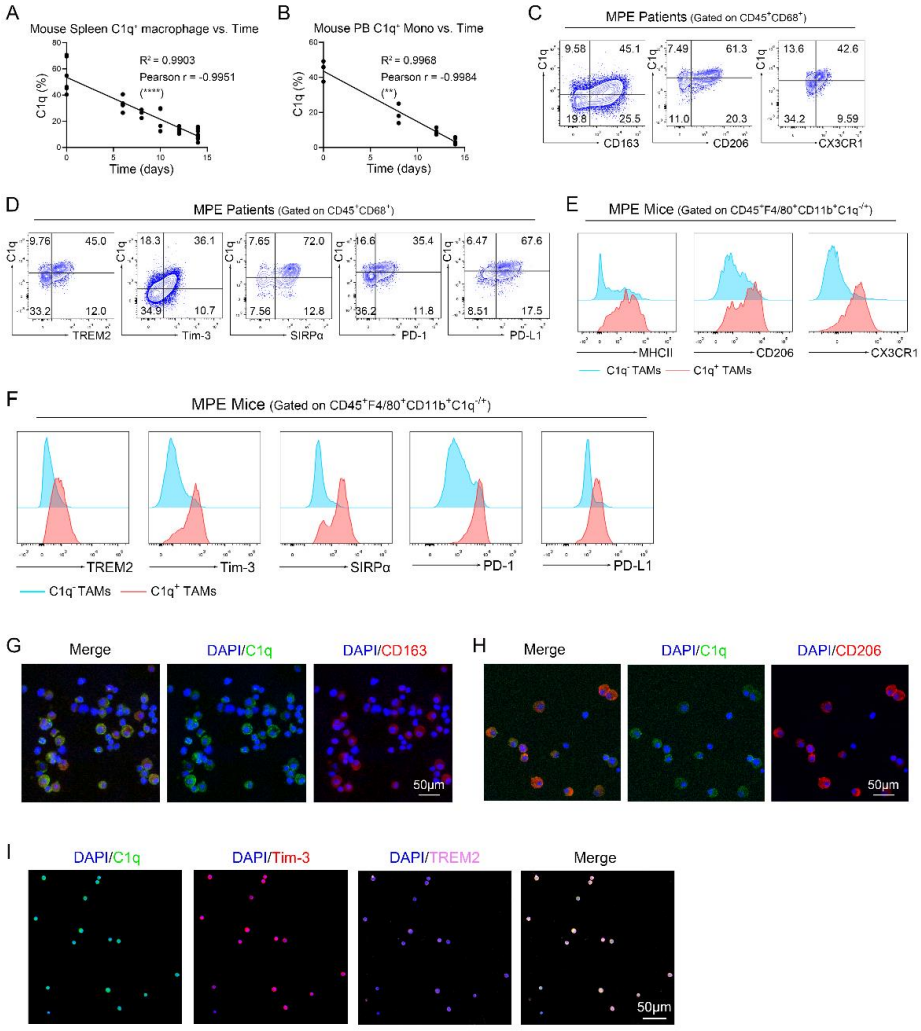

Figure S2. Related to Figure 2.

(A and B) The percentages of C1q^{+}macrophages in the spleen of MPE mice and C1q^{+}monocytes in the peripheral blood of MPE mice were measured at different time points using flow cytometry.

(C and D) Immune cells were isolated from human MPE, and flow cytometry was used to detect macrophage markers (CD163, CD206, CX3CR1) as well as inhibitory molecules (TREM2, Tim-3, SIRPα, PD-1, PD-L1).

(E and F) Immune cells were isolated from mouse MPE, and flow cytometry was used to detect macrophage markers (MHCII, CD206, CX3CR1) as well as inhibitory molecules (TREM2, Tim-3, SIRPα, PD-1, PD-L1).

(G and H) TAMs were isolated from human MPE using magnetic-activated cell sorting (MACS),

followed by immunofluorescence staining for C1q, CD163 (G), and CD206 (H) on TAMs. Green, C1q; Red, CD163/CD206; and blue, DAPI for nucleus. Scale bar 50 μm.

(I) TAMs were sorted from mouse MPE using MACS, followed by immunofluorescence staining for C1q, Tim-3, and TREM2 on TAMs. Green, C1q; Red, Tim-3; pink, TREM2; and blue, DAPI for nucleus. Scale bar 50 μm.

Data shown in (C)–(I) are representative of at least 3 mice (mean ± SD). Statistical analysis was performed using Pearson correlation coefficient (A, B). ** $P < 0.01$, **** $P < 0.0001$.

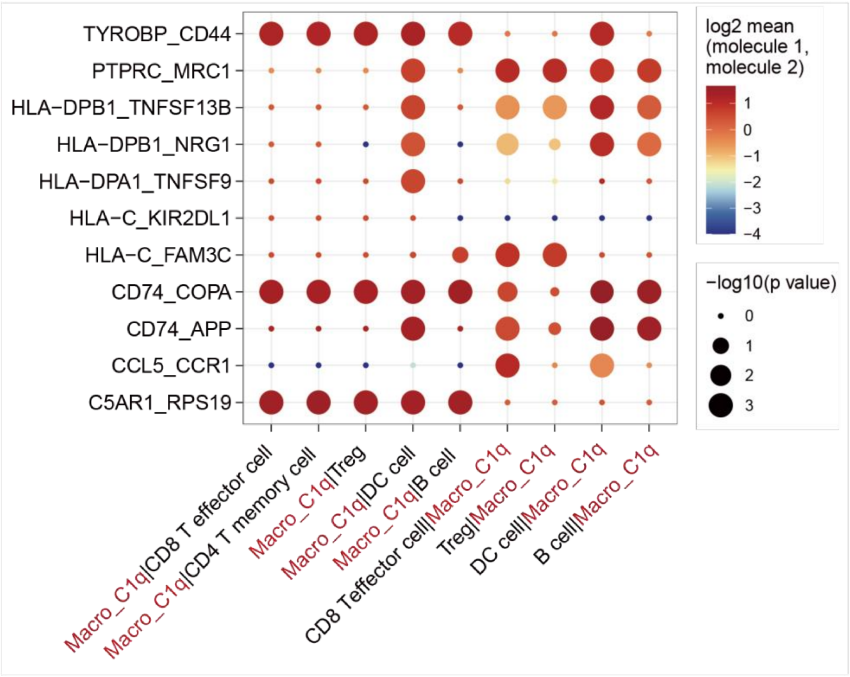

Figure S3. Interactions between cell subsets from scRNA-seq.

Bubble heatmap displays the average attraction strength of ligand-receptor pairs between $C1q^+$ macrophages and other cell subsets identified by scRNA-seq. Attraction strength was determined using CellPhoneDB, with dot size indicating the level of attraction strength and colors representing the *P* value calculated through permutation testing.

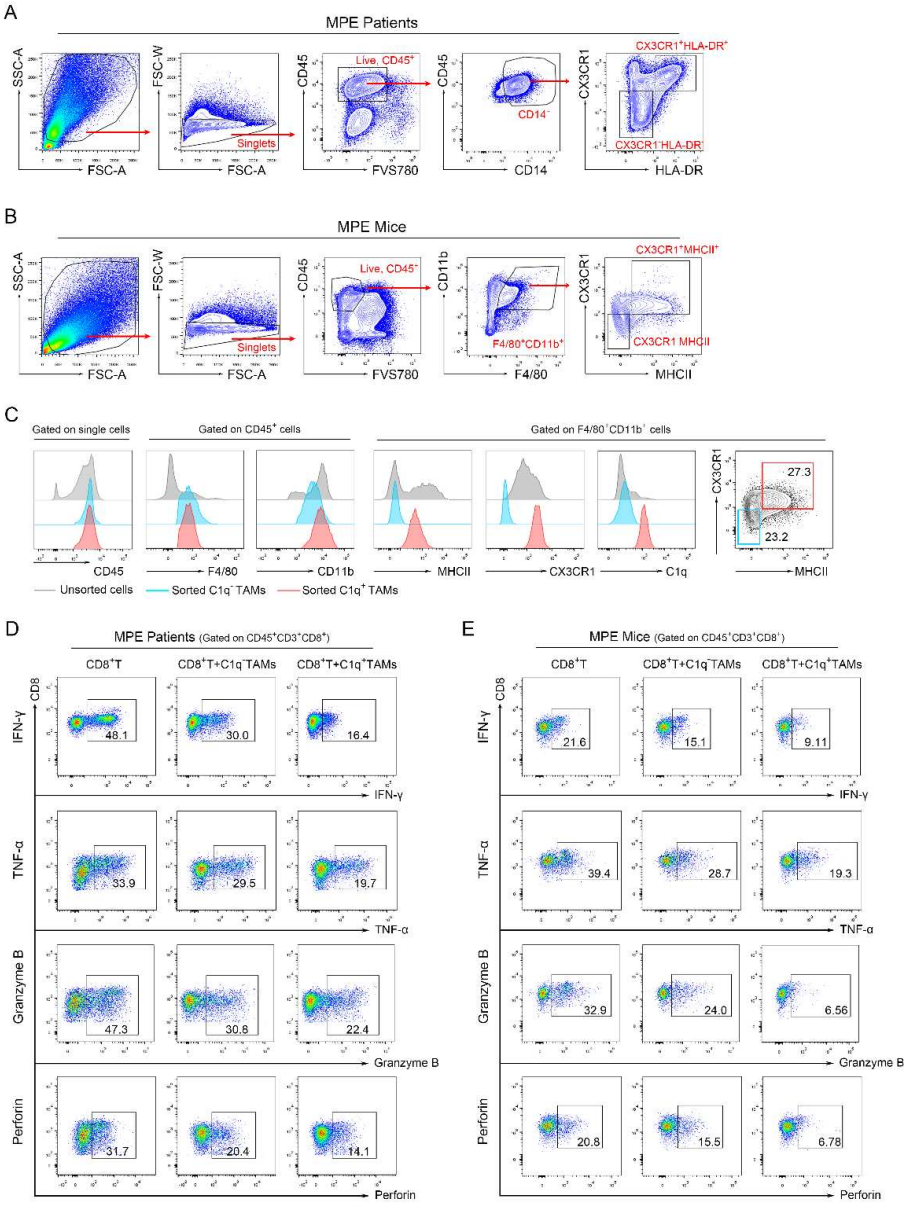

Figure S4. Related to Figure 3.

(A and B) Gating strategy of isolating human (A) and mouse (B) $C1q^+$ TAMs.

(C) The FACS efficiency of $C1q^+$ TAMs in mouse MPE was confirmed by C1q expression.

(D and E) $C1q^+$ and $C1q^-$ TAMs isolated from human (B) and mouse (C) MPE by FACS co-cultured with $CD8^+$ T cells isolated from peripheral blood of healthy donors (B) and mouse spleen (C) by MACS for 72 hours. Representative flow cytometry plots of IFN-γ, TNF-α,

granzyme B and perforin of $CD8^+$ T cells were shown.

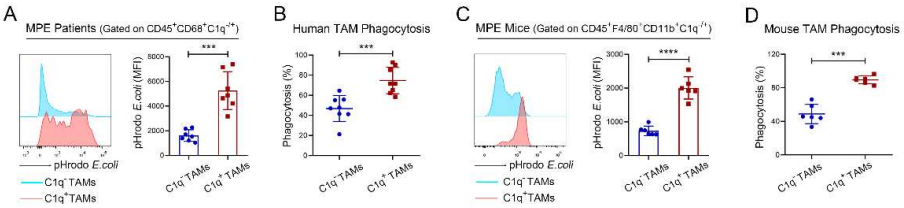

Figure S5. $C1q^+$TAMs exhibit stronger phagocytic ability.

(A–D) The phagocytic capacity of macrophages was detected using flow cytometry by phagocytosing pHrodo-labeled *E.Coli*. (A and B) TAMs in human MPE; (C and D) TAMs in mouse MPE.

Data shown in (A)–(D) are representative of at least three independent experiments (mean ± SD). Statistical analysis was performed using paired two-tailed Student's *t* test. *** $P < 0.001$, **** $P < 0.0001$.

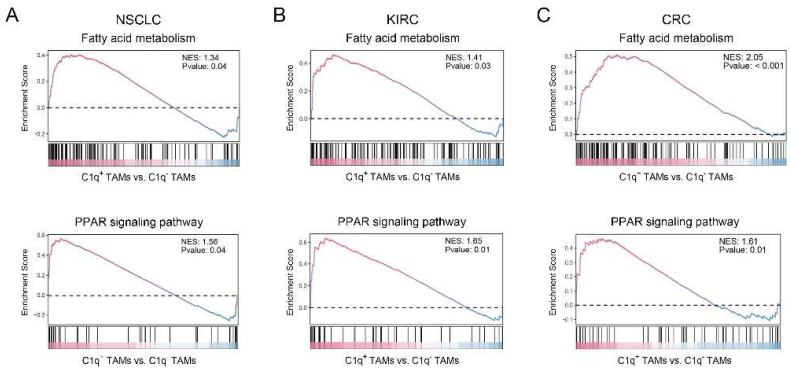

Figure S6. Related to Figure 4.

(A–C) Gene-set enrichment analysis (GSEA) was performed on genesets of fatty acid metabolism and PPAR signaling pathway in NSCLC, KIRC, and CRC. NES, normalized enrichment score. Positive NES indicate higher expression in $C1q^+$ TAMs.

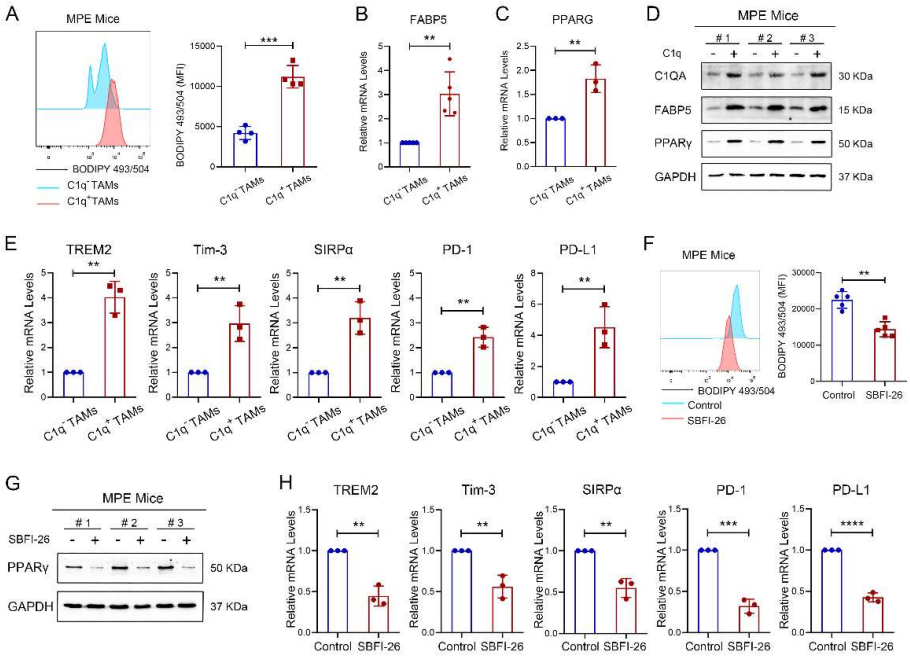

Figure S7. FABP5-mediated lipid metabolism programming in mouse C1q$^+$TAMs.

(A) Fatty acid accumulation of TAMs in mouse MPE was assessed by BODIPY 493/503 stain using flow cytometry.

(B and C) The relative expression levels of FABP5 and PPARG genes in sorted C1q$^+$ TAMs and C1q$^-$ TAMs from mouse MPE were measured by qRCR.

(D) The expression levels of C1q, FABP5, and PPARγ proteins in sorted C1q$^+$ TAMs and C1q$^-$ TAMs from mouse MPE were measured by Western blotting.

(E) The relative expression levels of TREM2, Tim-3, SIRPα, PD-1, and PD-L1 genes in sorted C1q$^+$ TAMs and C1q$^-$ TAMs from mouse MPE were measured by qRCR.

(F–H) TAMs of mouse MPE were treated with 100μM SBFI-26 or 0.1% DMSO for 72 hours. Fatty acid accumulation of mouse TAMs was assessed by BODIPY 493/503 stain using flow cytometry (F). The protein expression level of PPARγ in TAMs from mouse MPE was measured by Western blotting (G). The relative expression levels of TREM2, Tim-3, SIRPα, PD-1, and PD-L1 genes in TAMs from mouse MPE were measured by qRCR (H).

Data shown in (A)–(H) are representative of at least three independent experiments (mean ± SD). Statistical analysis was performed using paired two-tailed Student's *t* test (A–C, E) or unpaired

two-tailed Student's *t* test (F, H). ** $P < 0.01$, *** $P < 0.001$, **** $P < 0.0001$.

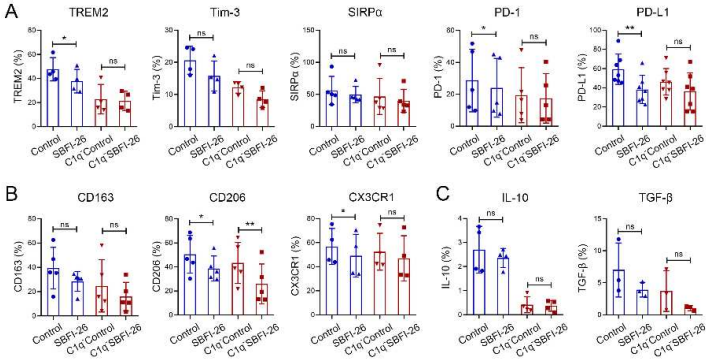

Figure S8. Related to Figure 5.

TAMs were sorted from human MPE and were treated with 100μM SBFI-26 (FABP5 inhibitor) or 0.1% DMSO for 72 hours.

(A) Immune inhibitory molecules (TREM2, Tim-3, SIRPα, PD-1, PD-L1) in total TAMs and C1q$^-$TAMs were detected by flow cytometry.

(B) M2-like markers (CD163, CD206, CX3CR1) in total TAMs and C1q$^-$ TAMs were detected by flow cytometry.

(C) The expression of IL-10 and TGF-β in total TAMs and C1q$^-$ TAMs were detected by flow cytometry.

Data shown in (A)–(C) are representative of at least 3 mice (mean ± SD). Statistical analysis was performed using unpaired two-tailed Student's *t* test. * $P < 0.05$, ** $P < 0.01$, ns: not statistically significant.

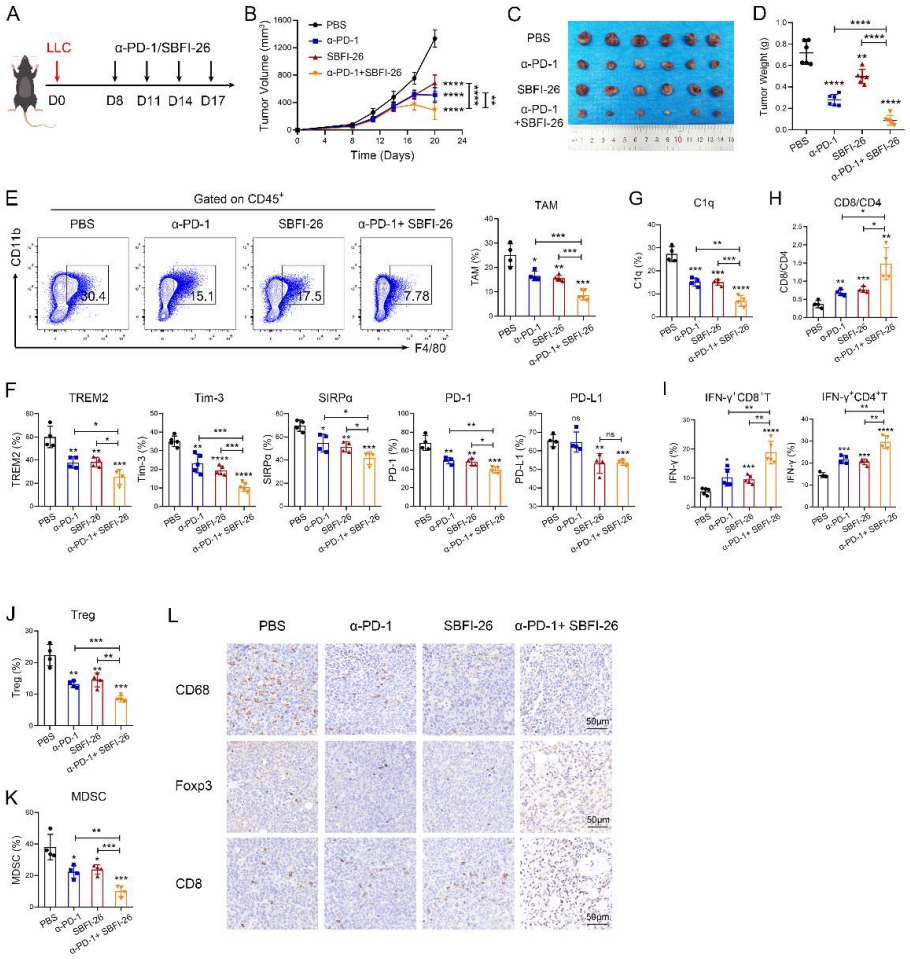

Figure S9. FABP5 inhibition alleviates immunosuppression and potentiates response to ICB therapy in lung cancer. Related to Figure 7.

(A–D) Schematic diagram of LLC subcutaneous xenograft tumor model. The tumor-burden mice were randomly assigned to four groups: mice with PBS, mice with anti-PD-1 antibody (α-PD-1), mice with SBFI-26, mice with α-PD-1 and SBFI-26 (A). Tumor volume growth curve (B), tumors in different groups (C), and Kaplan-Meier survival plot (D) were observed.

(E–K) Tumor-infiltrating immune cells were isolated from mouse subcutaneous tumors. The percentages of TAMs in immune cells (E), TREM2, Tim-3, SIRPα, PD-1, PD-L1 (F) and C1q (G) in TAMs, CD8/CD4 (H), IFN-γ^+CD8$^+$T cells and IFN-γ^+CD4$^+$T (I), Treg (J), and MDSC (K) were analyzed by flow cytometry.

(L) Paraffin-embedded sections of subcutaneous tumors were analyzed by CD68, Foxp3 and CD8

staining.

Data shown in (B)–(L) are representative of at least 3 mice (mean ± SD). Statistical analysis was performed using one-way ANOVA followed by Tukey's post hoc test. * $P < 0.05$, ** $P < 0.01$, *** $P < 0.001$, **** $P < 0.0001$, ns: not statistically significant.